

Supporting information for

Domain structure evolution in $\text{Ba}(\text{Zr}_{0.1}\text{Ti}_{0.9})\text{O}_3/(\text{Ba}_{0.75}\text{Ca}_{0.25})\text{TiO}_3$ multilayered thin films

For comparison, the end member of $(\text{Ba}_{0.75}\text{Ca}_{0.25})\text{TiO}_3$ and $\text{Ba}(\text{Zr}_{0.1}\text{Ti}_{0.9})\text{O}_3$ were also grown with the same substrate and deposition condition. As displayed in Figure S1 & S2, the BCT film has smaller grain size compared to BZT film. Compared to the multilayered BCT/BZT thin films, the end member of both BCT and BZT has inferior OP and IP contrast. As shown in Figure S3 & S4, the BCT and BZT show inferior switching behavior compared to multilayer thin films.

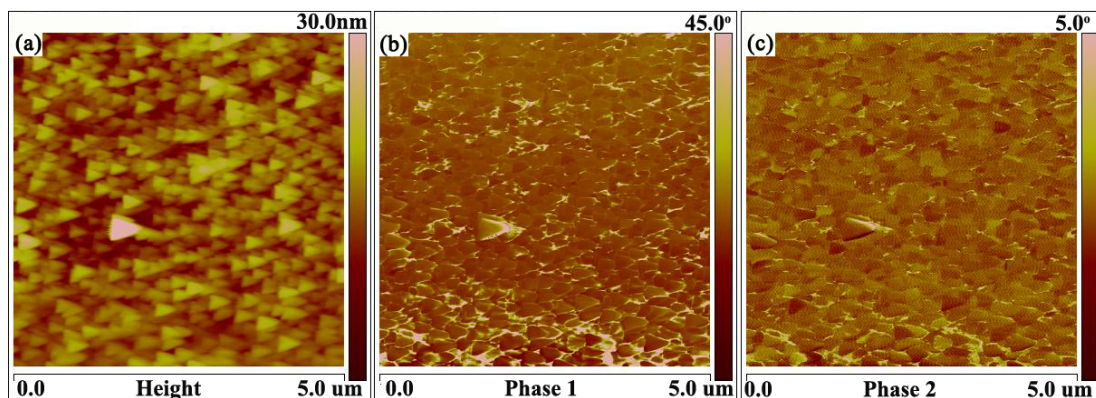


Figure S1. (a) Contact mode topography image, (b) OP-PFM phase image, and (c) IP-PFM phase images of domain structure of $\text{Ba}(\text{Zr}_{0.1}\text{Ti}_{0.9})\text{O}_3$ films.

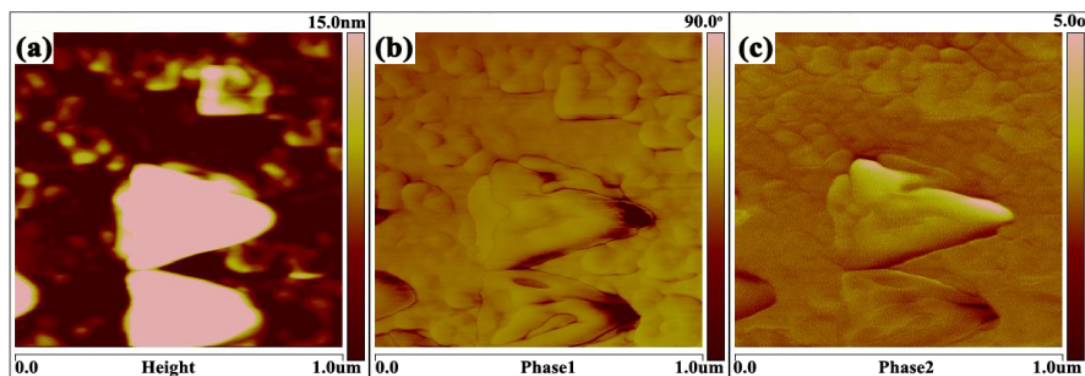


Figure S2. (a) Contact mode topography image, (b) OP-PFM phase image, and (c) IP-PFM phase images of domain structure of $(\text{Ba}_{0.75}\text{Ca}_{0.25})\text{TiO}_3$ films.

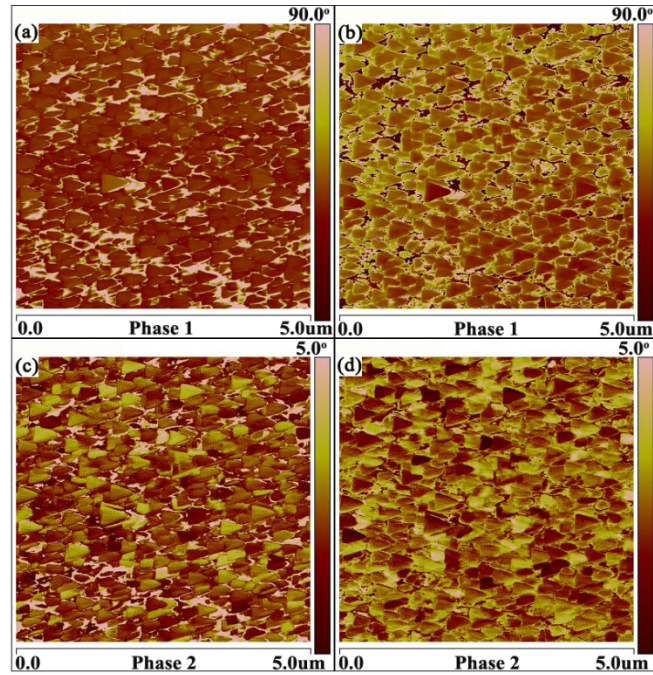


Figure S3. Out-of-plane phase image when (a) +10 V and (b) -10 V is applied to the sample surface, and in-plane phase image when (c) +10 V and (d) -10 V is applied to the $\text{Ba}(\text{Zr}_{0.1}\text{Ti}_{0.9})\text{O}_3$ sample surface, respectively.

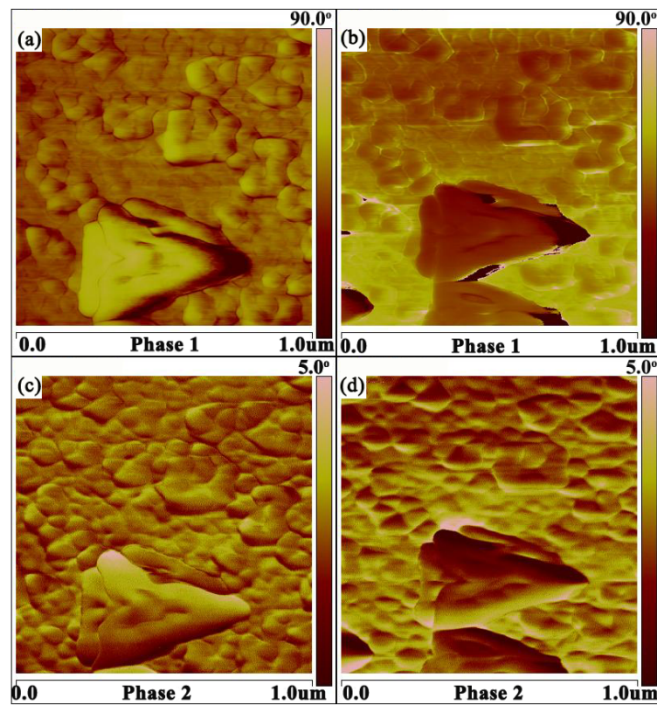


Figure S4. Out-of-plane phase image when (a) +10 V and (b) -10 V is applied to the sample surface, and in-plane phase image when (c) +10 V and (d) -10 V is applied to the $(\text{Ba}_{0.75}\text{Ca}_{0.25})\text{TiO}_3$ sample surface, respectively.

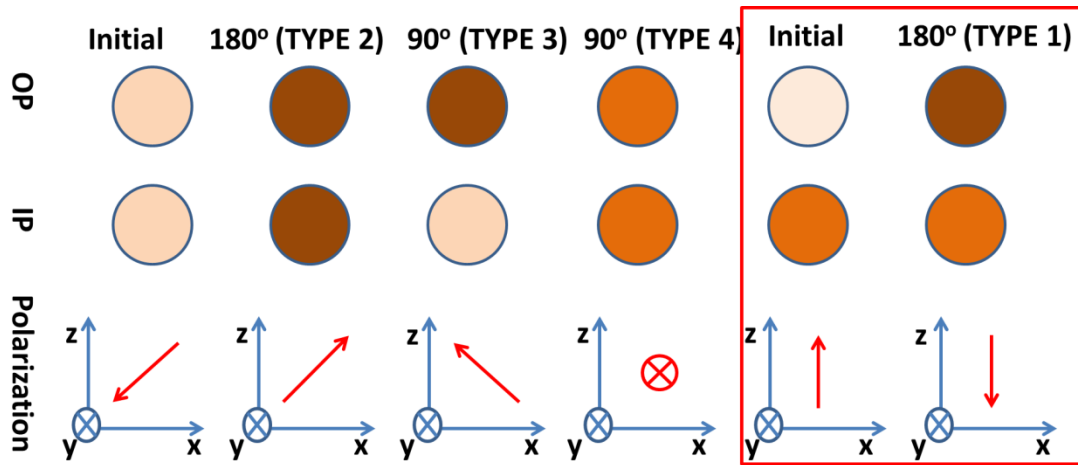


Figure S5. Schematic representation of individual domain switching displayed in OP signal (top row), and IP (middle row) signals. The bottom row shows the effective distribution of polarization vectors in each state. Note that type 3 and type 1 has similar initial state and switching signals.